Engineered Science
DOI: https://dx.doi.org/10.30919/es1148

Catalytically Active Cu-Fe/kaolin Hybrid Catalyst for Semi-Hydrogenation of Acetylene

Christiana Dupe Adegbesan,[1, 2] Samuel Daniel,[1, 2] Cedric Karel Fonzeu Monguen,[1, 4] Hannington Nevin Otieno[1, 2] and Zhen-Yu Tian[1, 2, 3,*]

Abstract

A series of Cu-Fe-base kaolin samples were prepared using the sol-gel method for semi hydrogenation of acetylene. The catalysts were comprehensively characterized with scanning electron microscope (SEM), X-ray diffraction (XRD), X-ray photoelectron spectroscopy (XPS) and H2-temperature programmed reduction (H_2-TPR). The rough structures of the catalysts support acetylene movement on the catalyst's surface and the desorption of ethylene. The catalysts promote ethylene selectivity and yield remarkably. The changes in the morphology of the modified kaolin with Cu-Fe improved the mass transport of reactants and products. The observed slight shift of the characteristic peak of Cu to a lower energy level in the XPS profile indicates changes in the electronic structure. These changes could stem from interactions of Cu with Fe and Kaolin or changes in the catalyst's surface. The prepared catalyst was tested for semi-hydrogenation of C_2H_2 within the temperature range of 100 to 200 ℃. In general, $Cu_xFe_{0.5}$/Kaolin catalysts exhibited good activity. The $Cu_3Fe_{0.5}$/kaolin ratio gave the highest yield, with >95% selectivity and >93% conversion, which is due to the shift in the Cu binding energy towards low energy which was more evident in this ratio. These results will enrich the use of non-precious metals as industrial catalysts for thermal conversion of C_2H_2 to ethylene.

Keywords: Semi-hydrogenation; Kaolin; Hybrid catalyst; non-precious metals; Cu-Fe catalyst.
Received: 03 January 2024; Revised: 12 March 2024; Accepted: 26 April 2024.
Article type: Research article.

1. Introduction

Ethylene (C_2H_4) is one of the most important precursors in the chemical industry[1-3] with an annual global demand of over 185 Mt.[4] It is used mainly as a precursor for polymers such as vinyl chloride, polyethylene, ethylene benzene, *etc*. C_2H_4 is a prominent intermediate in the synthesis of drugs, pesticides, and other valuable chemicals.[5] A high percentage of C_2H_4 is polymerized to form polyethylene; the rising demand for ethylene in the chemical industry is demonstrated by the diverse output of the end products from this product.[6]

The methods of producing C_2H_4 include naphtha stream cracking, dehydrogenation of saturated counterparts (ethane), ethanol dehydration, electrochemical conversion of greenhouse gases (mainly CO_2 and CH_4) and hydrogenation of acetylene. Hydrogenation catalysis stands as the basis of the chemical industry; it serves as one of its pillar reactions.[7,8]

Selective hydrogenation of acetylene (C_2H_2) to C_2H_4 without promoting further hydrogenation to ethane or other side reactions[9] is of high commercial importance. The separation of C_2H_2 from ethylene by traditional fractional distribution is not economically favorable because of the high energy demand. Thus, selective hydrogenation of C_2H_2 is also an appropriate method in the purification of ethylene in the C_2H_2 - C_2H_4 stream when C_2H_2 poses a threat for further use (such as polymerization) of C_2H_4 feedstock.[10] Selective catalytic hydrogenation requires a task-specific approach. The catalyst employed must allow high acetylene conversion, high

[1] *Institute of Engineering Thermophysics, Chinese Academy of Sciences, Beijing 100190, China.*
[2] *University of Chinese Academy of Sciences, Beijing 100049, China.*
[3] *State Key Laboratory of Coal Conversion, Institute of Engineering Thermophysics, Chinese Academy of Sciences, Beijing 100190, China.*
[4] *Institute for Chemical Technology and Polymer Chemistry, Karlsruhe Institute of Technology, Engesserstr. 20, Karlsruhe 76131, Germany.*
**Email:* tianzhenyu@iet.cn (Z-Y Tian)

© Engineered Science Publisher LLC 2024

selectivity concerning C_2H_4, high stability and regeneration, easy preparation and relatively low cost.[6] Over the years, suitable catalysts for the conversion of C_2H_2 to C_2H_4, such as Ni, Au, Pd, Cd, Ba, Ca, Zn, Mg, Ag, Cu, Fe, Pt, and Ir,[11-13] have been used. The conditions responsible for high performance have also been severely studied due to the industrial interest in ethylene. However, these catalysts have been reported to suffer from the formation of oligomer,[14] high activation energy,[15] and catalyst deactivation.[16,17]

Among other monometallic catalysts, Pd metal has shown outstanding activity of ≈ 97% C_2H_2 conversion. However, Pd has poor selectivity towards C_2H_4, S_{C2H4} ≈ 62%,[18] which led to the modification with Ag,[19] Ga,[20] Au,[21] Cu,[22,23] and Zn[24] using Al_2O_3, SiO_2, $CaCO_3$, TiO_2 *etc*. as support.[19] However, partial hydrogenation of acetylene appears challenging with Pd based-catalyst due to the formation of sub-surface H in the form of β-PdH, coke build-up on the active Pd sites and deactivation of catalysis during hydrogenation of C_2H_2.[25-27] Therefore, it is more realistic to search for stable catalysts that reduce the oligomer formation to the minimum, maximize the rate of ethylene formation, and enhance the ethylene desorption and at a relatively low cost.

Hybrid catalysts offer several advantages,[28] such as improved catalytic performance, increased stability, tunable selectivity, and stability. The essential components of hybrid catalysts can be synthetically controlled, investigated in a wide range of reaction conditions, and optimized to obtain the maximum catalytic performance. Cu is earth-abundant and has been severely studied as an electrocatalyst[29,30] and thermo-catalyst[31] for its high activity towards acetylene hydrogenation. Although Fe has been less commonly used for the semi-hydrogenation of acetylene, it nevertheless serves as a good promoter for Cu by increasing the activity of Cu. Here, kaolin is utilized due to its natural abundance, relatively inexpensive,[32] thermally stable and structural porosity. This porosity enhances the accessibility of reactants to the catalytic sites and dispersions of catalytic active sites, promoting efficient reaction kinetics and reducing mass transfer limitations. Precious metals are expensive, relatively scarce and sensitive to sulfur poisoning.[33] Photothermal hydrogenation of acetylene to ethylene using atomically dispersed Pd^{2+} on a nitrogen-doped graphene support has been reported with good conversion and selectivity.[34] However, utilization of precious metals as catalysts relatively increases the overall cost of C_2H_2 production. Therefore, there is a need to synthesize a relatively low-cost catalyst with high performance.

In this work, $Cu_xFe_{0.5}$/Kaolin was prepared using the sol-gel method with naturally abundant metals/materials to lower the production cost. The effect of varying Cu loading on kaolin was studied while keeping the Fe content constant. The choice of the hybrid catalyst in this work is not only for its high tendency for selective hydrogenation of acetylene but also for its low environmental toxicity and cost-effectiveness to pave the way for rational design of highly selective catalysts for acetylene hydrogenation to make more ethylene. The variation in the Cu loading and its interaction with Fe and the kaolin support was studied by characterizing the catalyst with techniques such as scanning electron microscope (SEM), X-ray diffraction (XRD), X-ray photoelectron spectroscopy (XPS) and H2-temperature programmed reduction (H2-TPR).

2. Experimental section

2.1 Catalyst preparation

Kaolin was purchased from Shanghai Macklin Biochemical Co., Ltd and was modified using NaOH. All precursors $(Fe(acac)_2$, 98.5% purity, procured from Sinopharm Chemical Reagent Co., Ltd and $Cu(acac)_2$, 97% purity, purchased from Macklin) were used as purchased with no further purification.

A series of $Cu_xFe_{0.5}$/Kaolin catalysts were prepared with different Cu loading using sol-gel method. To prepare 2% of Cu and 0.5% of $Fe(acac)_2$ loading in 10g of kaolin, 0.83 g of $Cu(acac)_2$ and 0.22 g Fe precursor were dissolved in ethanol with 10 g of base-modified kaolin as support. The mixture was stirred for 1 hour at room temperature, and ammonia solution was added both as a gel-forming agent and to adjust the pH of the mix. Citric acid was added as a complexing agent, and the mixture was stirred for another 2 hours at 60 ℃ temperature to ensure even distribution. After which, it was made to dry in an oven at 100 ℃ for 12 hours. The prepared catalyst was further calcined at 500 ℃ for 3 hours under air atmosphere. The as-prepared catalysts are designated as $Cu_xFe_{0.5}$/Kaolin, where x refers to the percentage loading of Cu. Subsequently, 3%, 4% and 5% were prepared according to the loading of Cu in kaolin while the amount of Fe is kept constant (0.22 g).

2.2 Characterization

To measure the crystalline structures of the catalysts, XRD was performed with the aid of a Rigaku, Tokyo, Japan, Ultima IV diffractometer with a Cu Kα monochromatized radiation (λ = 1.54056 Å) at a scanning speed of 0.05° s^{-1} within 2θ range of 5° to 90° at 40.0 mA, and 40.0 kV. The results were analyzed using PANalytical X'Pert Pro. JEOL-JSM-7800F prime-LV high-resolution microscope with acceleration voltages of 25.0 kV was used to investigate the morphology of the catalyst. XPS was recorded on an ESCALAB 250 spectrometer (Thermo Fisher Scientific, Al *Kα*, *hν* =1486.6 eV) under a vacuum of ~2×10^{-7} Pa and a spot size of 500.0μm, for

 © Engineered Science Publisher LLC 2024

ionic and elemental composition of the prepared catalyst. H_2-TPR was performed to analyze the reducibility of the catalysts. A 0.09 g sample was placed in a quartz reactor connected to a conventional TPR apparatus. The reactor was heated from 50 - 900 ℃ at a heating rate of 10 ℃/min, and a thermal conductivity detector (TCD) was used to measure the amount of H_2 uptake during the reduction. NH_3-TPD was also performed to ascertain the surface acidity of the catalyst.

2.3 Catalytic test

Selective hydrogenation of C_2H_2 was performed using a fixed-bed reactor. 0.2 g of the $Cu_xFe_{0.5}$/Kaolin catalyst was loaded in the center of a quartz tube guided by silica wool on both sides. The catalyst was reduced in H_2/He at 250 ℃ for 30 minutes. In this study, a gas mixture of C_2H_2, C_2H_4, H_2 and He in the ratio of 1:10:10:79 was used as feedstock, making a total flow rate of 50 SCCM controlled with Mass flow controllers. The products were analyzed at different temperatures such as 100 ℃, 125 ℃, 150 ℃, 175 ℃, and 200 ℃. The products were analysed by an online gas chromatograph (GC), and a flame ionization detector (FID) was used to detect and quantify the product separated by the chromatographic column.

The conversion of acetylene ($X_{acetylene}$), selectivity of ethylene ($S_{ethylene}$) and yield (Y_i) were calculated using:

$$X_{acetylene} = \frac{C_2H_2(in) - C_2H_2\,(out)}{C_2H_2\,(in)} \times 100 \quad (1)$$

$$S_{ethylene} = \left(1 - \frac{\sum Pi}{C_2H_2\,(feed) - C_2H_2}\right) \times 100 \quad (2)$$

$$Y_i = \frac{X_{acetylene} \times S_{ethylene}}{100} \quad (3)$$

3. Result and discussion

3.1 Phase Identification

XRD analysis was conducted to show the crystal pattern of the prepared catalysts. As shown in Fig. 1, the prominent diffraction peaks for kaolin (Aluminum silicon oxide) appeared at 2θ of 16.4°, 25.9°, and 26.2° (PDF# 01-082-0037). After CuFe was loaded, a sharp crystalline peak of CuO, monoclinic with a space group of C2/c (PDF# 01-089-2530) emerged at 2θ of 35.2°, 35.5°, 38.5°, 38.9° and 48.7° corresponding to the crystal planes of (-111), (002), (111), (200), and (-202) respectively. While Fe_2O_3 peaks (PDF# 01-073-0603), rhombohedral with space group R-3c corresponding to the crystal plane of (110), whose peak overlapped at 2θ of 35.6° with that of CuO was highly dispersed in all prepared catalyst. The sharp and narrow peaks observed indicate a good crystallinity level and that Cu_xFe/kaolin was synthesized successfully. A similar XRD profile obtained here was observed in the work where FeCu/Kaolin was used as an electrode.[35]

3.2 Morphology

It was shown in the SEM image (Fig. 2) that Cu_xFe/kaolin of different Cu loadings synthesized under similar conditions have slightly different morphologies. The difference in morphology of the catalysts was seen as an increase in superficial roughness from pure kaolin in Fig. 2a to the modification with Cu_xFe (Figs. 2b, c, d and e). This increased roughness promotes better contact between the catalyst, reactant and product. Thereby, facilitating mass transport of reactants to active sites and the removal of products from the catalyst surface.[36] The irregularities in the surface possibly create a pathway for the interaction between the reactants, the active sites and the product desorption, thus enhancing catalytic efficiency. The results from the SEM-EDS agree with that of the XRD profile, confirming that $Cu_xFe_{0.5}$/Kaolin was successfully synthesized. The irregularity in the shape of the catalyst as seen in the SEM image coupled with the surface roughness, could be a contributing factor facilitating mass transport of reactants to active sites and the removal of products from the catalyst surface, thereby, improving mass transport of reactants and products.

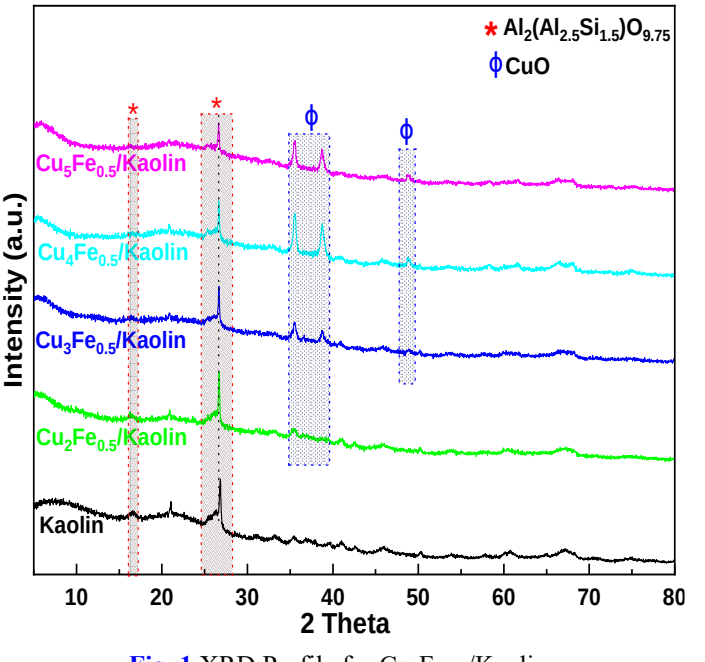

Fig. 1 XRD Profile for $Cu_xFe_{0.5}$/Kaolin.

3.3 Composition and ionic states

XPS spectra peak of Cu 2p was deconvoluted to correspond to the binding energy of electrons in the Cu 2p3/2 and Cu 2p1/2 energy level at 933.63 - 934.74 eV and 953.18 - 954.46 eV, respectively.[37] The characteristic peak of Cu was observed to shift slightly to a lower energy level; this is more evident in $Cu_3Fe_{0.5}$/Kaolin. The observed slight shift to a lower energy

© Engineered Science Publisher LLC 2024

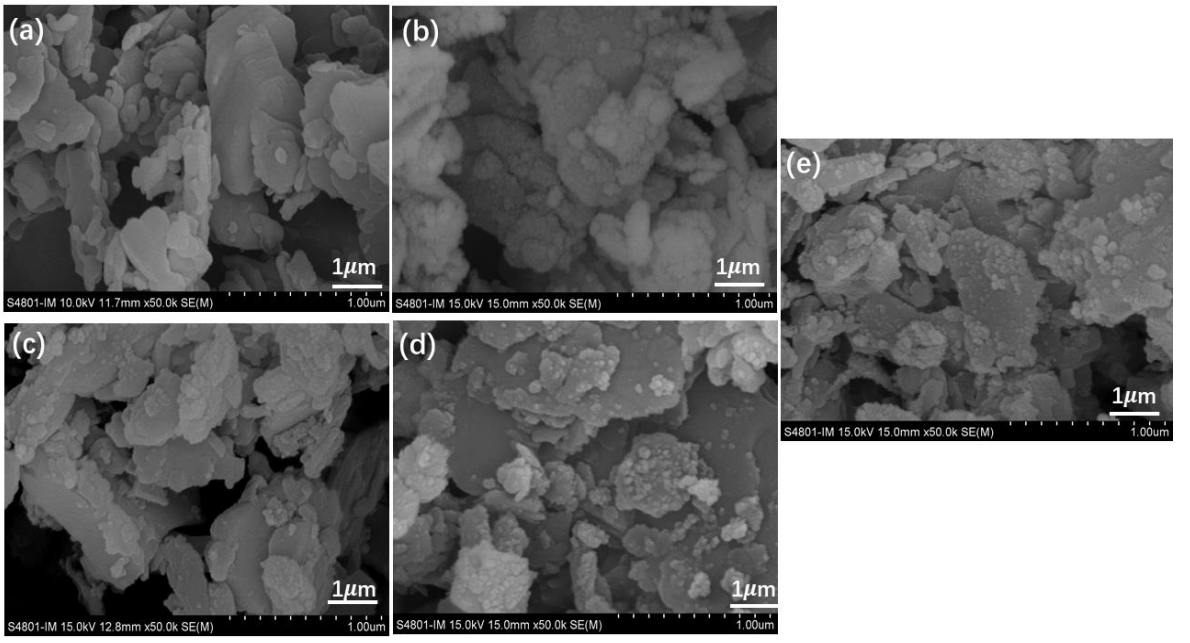

Fig. 2 SEM Image (a) kaolin; (b) Cu_2/kaolin; (c) $Cu_3Fe_{0.5}$/kaolin; (d) $Cu_4Fe_{0.5}$/kaolin; (e) $Cu_5Fe_{0.5}$/kaolin.

level indicates changes in the electronic structure; also, the reduction could stem from interactions of Cu with Fe and Al-Si in kaolin or changes in the catalyst's surface environment. Furthermore, the 3d orbital of Fe is partially filled, Cu could act as an electron donor because of the partially filled 4*s* band. In a Cu-Fe alloy, electrons could flow from Cu to Fe, leading to an orbital hybridization. The orbital hybridization can be said to influence the electronic structure of active sites. This fact is in agreement with the orbital hybridization theory. Cu 2p3/2 peaks of Cu_xFe/Kaolin samples shift slightly to a lower binding energy of 934.85 eV. The $Cu_3Fe_{0.5}$/Kaolin also shows the highest ratio of Cu^{2+} among the prepared catalysts (Table 1). The XPS signal from the Fe 2p core level in Cu_xFe/Kaolin samples is shown in Fig. 3b. The Fe 2p XPS signal was deconvoluted into the Fe 2p1/2 at 723.56 ± 1 eV and Fe 2p3/2 at 713.69 ± 1 eV. At 2% Cu loading, the ratio of Fe 2p1/2 was found to decrease with increasing Cu loading but then increased at 5% Cu loading. Serrano *et al*. explained that both Fe 2p1/2 and Fe 2p3/2 play roles as catalyst promoters in the semi-hydrogenation of acetylene to ethylene and both can act as active sites for the hydrogenation of acetylene to ethylene.[38]

3.4 Redox properties

Hydrogen Temperature-Programmed Reduction was used to study the reducibility of metal oxide species in the prepared $Cu_xFe_{0.5}$/Kaolin catalyst by monitoring their reaction with hydrogen gas at different temperatures. It gave insights into the redox properties of the catalyst and the interactions amongst the metal species and the support, as shown in Fig. 4. A broad undefined peak at about 45 °C to 668 °C was

Table 1. XPS analysis of $Cu_xFe_{0.5}$/Kaolin.

Catalysts	Elemental status	Cu 2p3/2		Cu 2p1/2		Fe 2p1/2		Fe 2p3/2
	Species	Cu^{2+}	Satellite	Cu^{2+}	Satellite	Fe^{2+}	Satellite	Fe^{3+}
$Cu_2Fe_{0.5}$/Kaolin	BE (eV)	934.74	942.85	954.46	962.71	723.56		713.69
	Area	15947.50	9068.03	8789.97	5750.59	7755.35		5785.33
	RA (%)	63.75	36.25	60.45	39.55	57.27		42.73
$Cu_3Fe_{0.5}$/Kaolin	BE (eV)	933.63	941.89	953.18	961.81	724.82	716.61	711.76
	Area	11625.60	5967.78	4971.81	3616.67	10492.30	5754.79	10774.3
	RA (%)	66.08	33.92	57.89	42.11	38.82	21.29	39.89
$Cu_4Fe_{0.5}$/Kaolin	BE (eV)	933.72	942.42	953.51	962.11	725.05	715.90	711.49
	Area	9041.68	5070.61	4847.05	4842.35	6963.87	6497.91	6911.41
	RA (%)	64.07	35.93	50.03	49.97	34.18	31.89	33.93
$Cu_5Fe_{0.5}$/Kaolin	BE (eV)	933.82	942.09	953.45	961.85	724.32	716.66	711.89
	Area	8500.43	5112.25	3769.28	2355.99	10277.50	1406.03	8908.78
	RA (%)	62.44	37.56	61.54	38.46	49.91	6.83	43.26

© Engineered Science Publisher LLC 2024

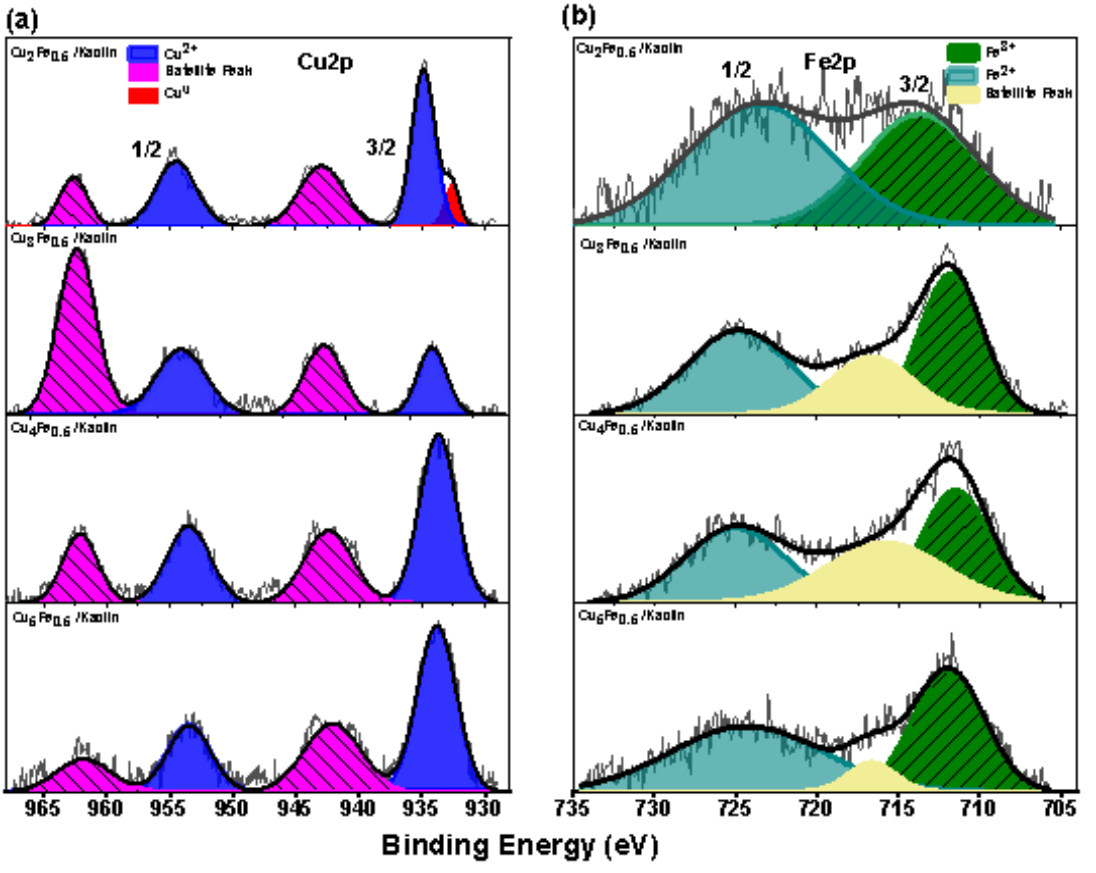

Fig. 3 XPS deconvolution of (a) Cu 2p and (b) Fe 2p of $Cu_xFe_{0.5}$/Kaolin samples.

observed with kaolin. However, after adding CuFe, a shift to lower temperature was observed for $Cu_2Fe_{0.5}$/kaolin with two peaks at 290 °C and 370 °C corresponding to CuO and Fe_2O_3 peaks respectively. However, as the loading of Cu increased from 2% to 3%, a further shift to a lower temperature with a sharp peak was observed, indicating that copper oxide reduction was promoted with well-dispersed Fe_2O_3. The shift to a lower temperature peak suggests that additional copper created more easily reducible species on the support's surface. It also shows a strong interaction between Cu and Fe species, forming intermetallic compounds.[39] The broad, partially defined peak observed for Cu_2Fe might indicate the synergistic effects of copper and iron on the redox properties of the $Cu_xFe_{0.5}$/Kaolin catalyst. The changes in peak positions, intensities, and broadening indicate the complex interactions between the metal species and their effects on the catalyst's reducibility. The H_2-TPR result agrees with the XRD result, showing a well-dispersed Fe_2O_3 at Cu loading greater than 2%.

3.5 Surface acidity

The surface acidity distribution and strengths of the $Cu_xFe_{0.5}$/Kaolin catalyst samples were determined by analyzing their acidic properties using NH_3-TPD analysis. The NH_3 desorption peaks were observed at 167 °C, 284 °C, and 508 °C. These peaks were categorized as weak, medium, and strong acid sites, respectively.[40] The distribution of acid sites varies with Cu loading. As observed from the NH_3-TPD profile in Fig. 5, the weak acidic site observed in kaolin support shifted to a lower temperature from 166 °C to 150 °C after 2% Cu was added. Although there was a slight shift towards high temperatures observed at 3% Cu, the density of acidic sites on the catalyst surface in the weak acidic site was the highest at this Cu concentration. A decrease in temperature towards the weak acidic site was observed with increasing Cu loading. The broad peaks observed indicate higher number of sites. The peak at the weak acidic sites could facilitates the adsorption/desorption of acetylene, the medium and strong acidic sites can activate the acetylene molecule for hydrogenation. The presence of different acidity strengths allows for selective activation of acetylene while minimizing undesired side reactions.[41] According to the reports, the presence of acid sites with lower strength facilitates the desorption of the product. A notable example is observed in the Fe/ZSM-12 catalyst, which exhibits relatively weaker surface acidity, resulting in rapid desorption of ethylene upon its formation. This observation highlights the influence of the catalyst surface acidity on the binding affinity of the ethylene product.[40]

© Engineered Science Publisher LLC 2024

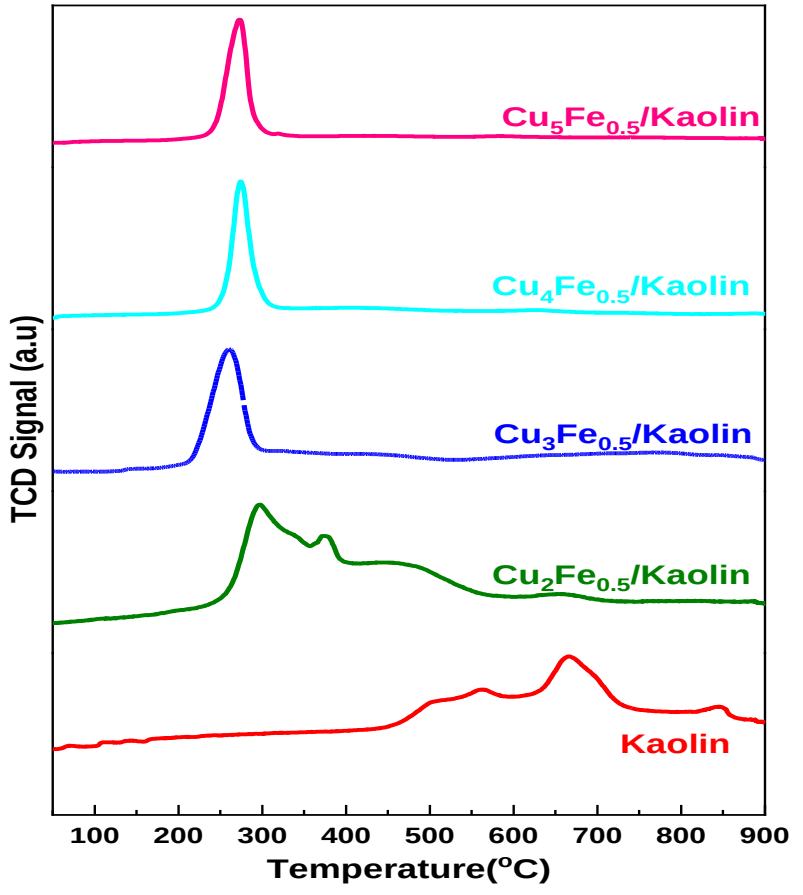

Fig. 4 H_2-TPR Profiles of $Cu_xFe_{0.5}$/Kaolin.

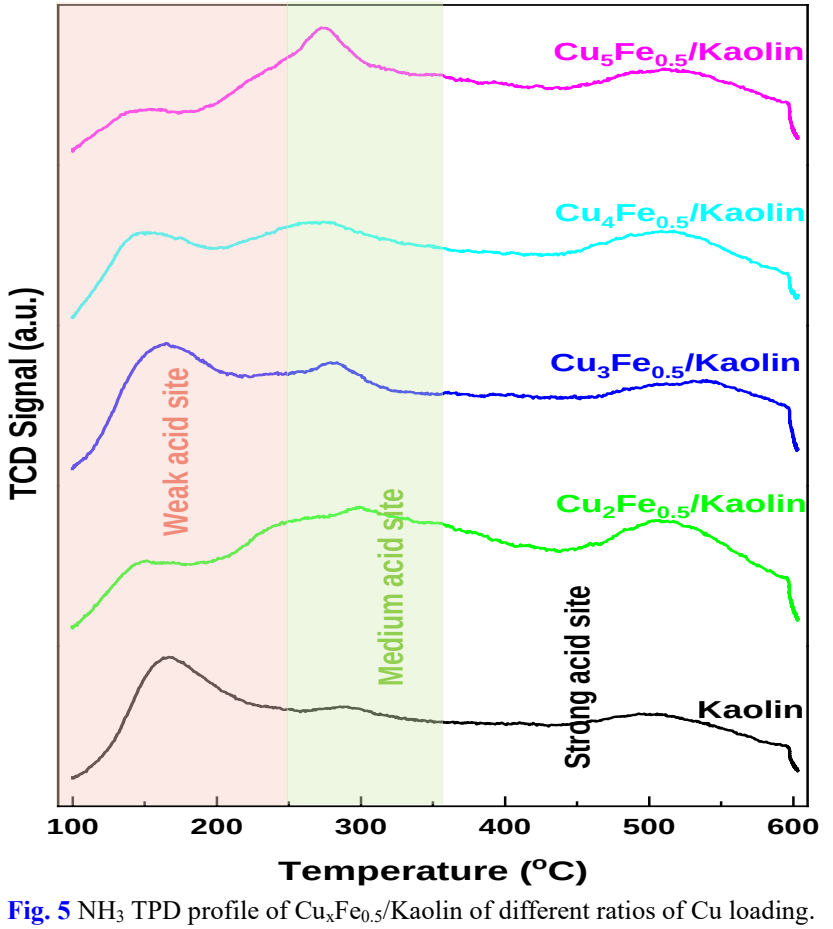

Fig. 5 NH_3 TPD profile of $Cu_xFe_{0.5}$/Kaolin of different ratios of Cu loading.

© Engineered Science Publisher LLC 2024

4. Catalytic performance

4.1 Effect of temperature and metal loading on catalyst performance

Acetylene conversion increased with increasing temperature, as shown in Fig. 6a. The Cu and Fe oxides within the catalyst displayed a synergistic effect, which ultimately led to an enhancement in conversion rates to a maximum. Nevertheless, the introduction of additional Cu loading resulted in a subsequent decrease in conversion rates. To achieve a better understanding of the relationship between the structures of the catalysts and the catalytic performances, the influence of the Cu_xFe atomic ratios on the catalyst's conversion, selectivity, and yield was shown in Fig. 6b. It is worth noting that the highest conversion (93.27%), selectivity (95.79%) and yield (89.34%) was observed with Cu loading of 3% ($Cu_3Fe_{0.5}$/kaolin) at 200 °C.

The effect of Cu loading on $Cu_xFe_{0.5}$/kaolin was studied at 200 °C and demonstrated in Fig. 6c. The percentage conversion of C_2H_2 increased from 27.18% with kaolin to a maximum of 93.27% with $Cu_3Fe_{0.5}$/kaolin, after which acetylene conversion started decreasing with further loading of Cu. A similar trend of rising and falling with an increase in Cu loading was observed with the percentage selectivity of the desired product.

In Fig. 7 shows a decrease in selectivity as the temperature rises from 100 °C to 200 °C. This phenomenon occurs because as the temperature increases, the proportion of side products obtained from the reaction using Cu_xFe/kaolin becomes significant. Notwithstanding, a selectivity of 95.79% was observed at 200 °C for $Cu_3Fe_{0.5}$/kaolin. A graph of selectivity of all products (desired and by-products (Fig. 6d)) obtained was also plotted. The percentage of 1,3-butadiene was observed to be the highest competing by-product with a maximum value of 5% at 5% Cu loading and 6% on kaolin support.

Higher acetylene conversion was achieved at higher temperatures, but as the increase in the main reaction rate was observed, it enhanced the rate of side reactions. This trend was also reported in previous studies.[27]

4.2 Comparison with other literature

The activity of the catalyst in this work was compared to those from previous works. The activity of $Cu_3Fe_{0.5}$/kaolin was competitive with the conversion and selectivity of other work containing the precious metal catalyst. Although 100% conversion has been achieved using $Pd_2Ga_{1-x}Sn_x$[42] and Pd_1/ND@G)[43] as shown in Fig. 8 nevertheless, the synthesis of these catalysts involves the use of precious metal, which

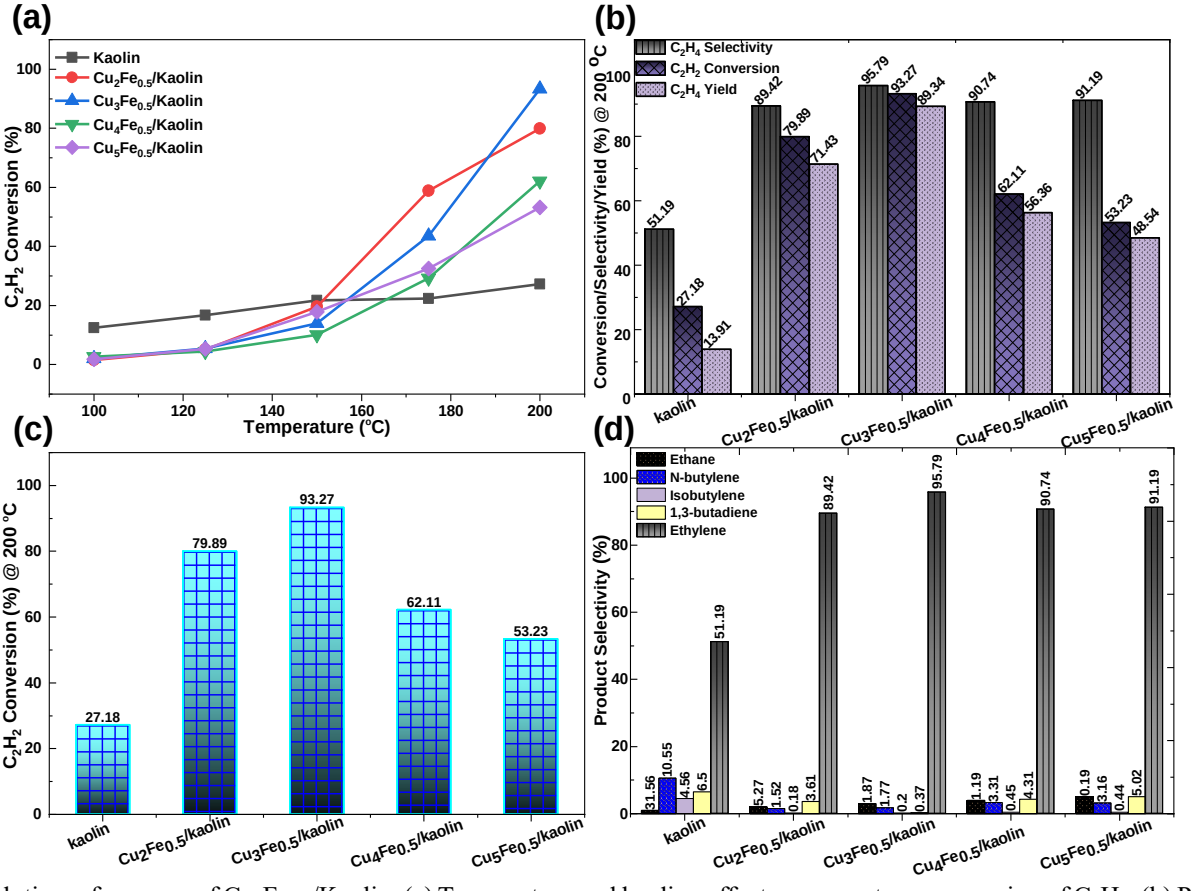

Fig. 6 Catalytic performance of $Cu_xFe_{0.5}$/Kaolin: (a) Temperature and loading effect on percentage conversion of C_2H_2; (b) Percentage conversion, selectivity and yield at 200 °C; (c) conversion at 200 °C; (d) Selectivity of desired and by-products at 200 °C.

© Engineered Science Publisher LLC 2024

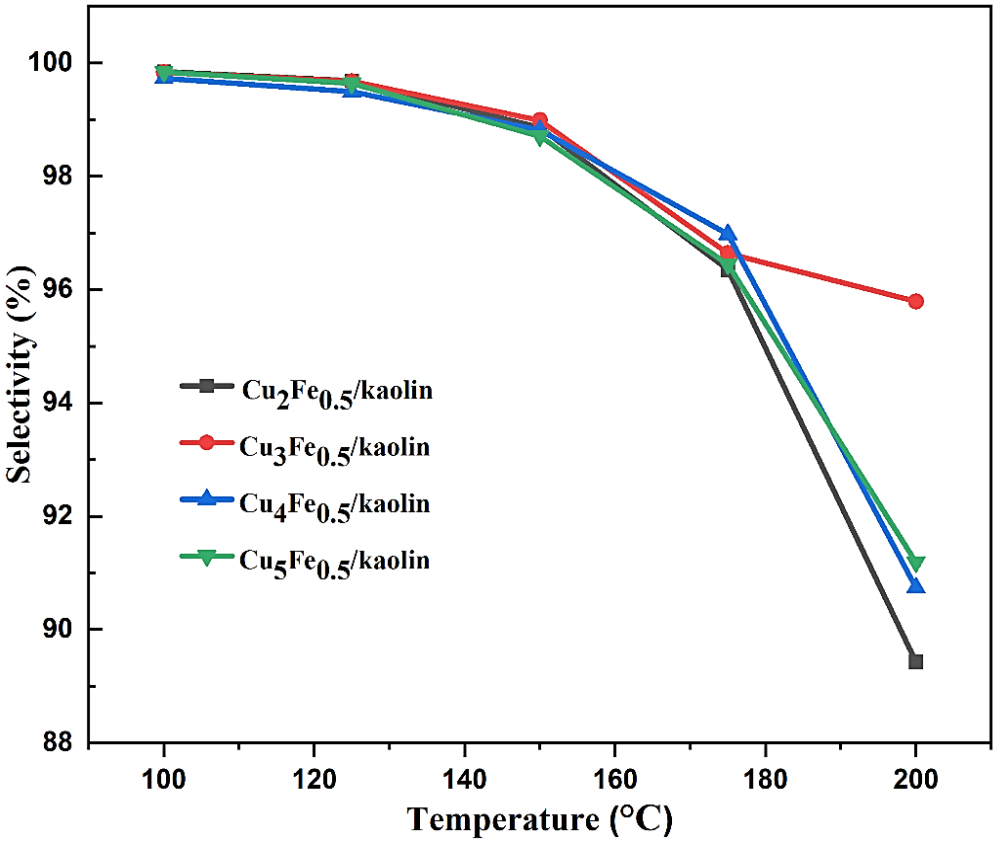

Fig. 7 Ethylene selectivity against temperature.

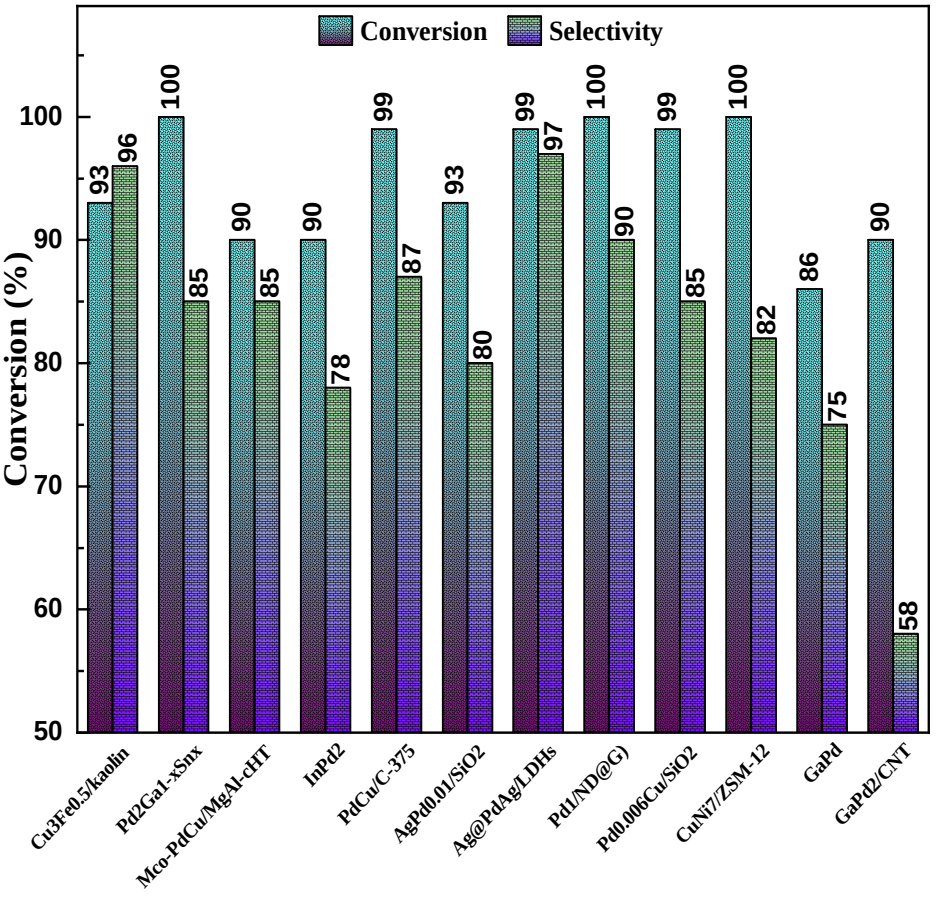

Fig. 8 Comparison of the activity of Cu_xFe/Kaolin with those of $Pd_2Ga_{1-x}Sn_x$,[42] Mco-PdCu/MgAl-cHT,[44] $InPd_2$,[45] PdCu/C-375,[46] $AgPd_{0.01}/SiO_2$,[47] Ag@PdAg/LDHs,[48] Pd_1/ND@G),[43] $Pd_{0.006}Cu/SiO_2$,[49] $CuNi_7$/ZSM-12,[40] GaPd,[50] $GaPd_2$/CNT.[51]

© Engineered Science Publisher LLC 2024

might result in an overall high cost of ethylene production.

It is worth noting that almost all catalysts alloyed with Pd had achieved the semi-hydrogenation of acetylene at a lower temperature, which is commendable; however, Pd is toxic, and the aim is to design a catalyst that is relatively inexpensive and environmentally benign. $CuNi_7$/ZSM-12,[40] had also given a conversion of 100% at 250 °C but the selectivity is not as high as the selectivity obtained in this work, coupled with the fact that Ni is relatively toxic.

5. Reaction mechanism

C_2H_2 comes near the active site of $Cu_xFe_{0.5}$/Kaolin by adsorbing onto the catalyst's surface; the triple bond in acetylene interacts with metal sites on the catalyst surface. Hydrogen (H_2) molecules also adsorb onto the catalyst surface and migrate to the adsorbed acetylene. One hydrogen atom is added to one carbon of the C_2H_2, forming a vinyl intermediate.

$H_2(g) + Cu_xFe/kaolin(s) \rightarrow 2H[Cu_xFe/kaolin]$

$C_2H_{2(g)} + Cu_xFe/kaolin(s) \rightarrow C_2H_2[Cu_xFe/kaolin]$

$C_2H_2[Cu_xFe/kaolin] + H[Cu_xFe/kaolin] \rightarrow C_2H_3[Cu_xFe/kaolin]$

$C_2H_3[Cu_xFe/kaolin] + H[Cu_xFe/kaolin] \rightarrow C_2H_4[Cu_xFe/kaolin]$

$C_2H_4[Cu_xFe/kaolin] \rightarrow C_2H_{4(g)} + Cu_xFe/kaolin$

The vinyl intermediate undergoes further hydrogenation with another hydrogen atom adding to the vinyl intermediate on the surface of Cu_xFe/kaolin, forming ethylene. Ethylene and hydrogen desorb from the catalyst's surface, limiting further hydrogenation, thereby supporting high selectivity. The unique structure of the catalyst ensures the easy adsorption of acetylene on the surface of Cu_xFe/kaolin and the desorption of ethylene from the catalyst's surface, promoting plausible and remarkable selectivity and yield of ethylene rather than excess hydrogenation to ethane. The formation of higher hydrocarbons is neglected in the mechanism of this work because the by-products formed are negligible. Horiuti–Polanyi mechanism[52] has been used to describe the mechanism in this work.

6. Conclusion

$Cu_xFe_{0.5}$/Kaolin catalyst was successfully synthesized for the semi-hydrogenation of acetylene to ethylene. The effect of Cu loading and its interaction with kaolin support was studied by characterizing the catalyst with techniques such as SEM, XRD-EDS, XPS, H_2-TPR and NH_3-TPD techniques. This characterization gave insight into the structure and morphological changes with increased Cu loading. Changes in ionic states, electronic and binding energy were evident, as well as redox properties of Cu_xFe/Kaolin. The as-synthesized $Cu_3Fe_{0.5}$/kaolin catalyst not only demonstrates a highly competitive activity compared with the usage of precious metals such as Pd and Ag but also shows high activity for acetylene semi-hydrogenation and remarkable selectivity of > 95 towards ethylene, leading to increased yield. The relatively high selectivity obtained in this research could be attributed to ethylene desorption from the catalytic active sites of $Cu_xFe_{0.5}$/kaolin catalyst. The further hydrogenation of ethylene to ethane was suppressed due to the absence of a hydrogen spill reservoir in the $Cu_xFe_{0.5}$/kaolin catalyst.

Acknowledgements

ZY Tian thanks the financial support from the National NSFC (No. 52325604), MOST (2021YFA0716200/2022YFB4003900), National Major Science and Technology Projects of China (J2019-III-0005-0048). C. D. Adegbesan, S. Daniel, C.K. Fonzeu Monguen and H. N. Otieno acknowledge the financial support of ANSO.

Conflict of Interest

There is no conflict of interest.

Supporting Information

Not applicable.

References

[1] L. S. Layritz, I. Dolganova, M. Finkbeiner, G. Luderer, A. T. Penteado, F. Ueckerdt, J.-U. Repke, The potential of direct steam cracker electrification and carbon capture & utilization via oxidative coupling of methane as decarbonization strategies for ethylene production, *Applied Energy*, 2021, **296**, 117049, doi: 10.1016/j.apenergy.2021.117049.

[2] J.-M. Chen, B. Yu, Y.-M. Wei, Energy technology roadmap for ethylene industry in China, *Applied Energy*, 2018, **224**, 160-174, doi: 10.1016/j.apenergy.2018.04.051.

[3] C. W. Fernelius, H. Wittcoff, R. E. Varnerin, Ethylene: the organic chemical industry's most important building block, *Journal of Chemical Education*, 1979, **56**, 385, doi: 10.1021/ed056p385.

[4] R. Huang, M. Xia, Y. Zhang, C. Guan, Y. Wei, Z. Jiang, M. Li, B. Zhao, X. Hou, Y. Wei, Q. Chen, J. Hu, X. Cui, L. Yu, D. Deng, Acetylene hydrogenation to ethylene by water at low temperature on a Au/α-MoC catalyst, *Nature Catalysis*, 2023, **6**, 1005-1015, doi: 10.1038/s41929-023-01026-y.

[5] C. Urmès, J.-M. Schweitzer, A. Cabiac, Y. Schuurman, Kinetic study of the selective hydrogenation of acetylene over supported palladium under tail-end conditions, *Catalysts*, 2019, **9**, 180, doi: 10.3390/catal9020180.

[6] S. A. Nikolaev, L. N. Zanaveskin, V. V. Smirnov, V. A. Averyanov, K. L. Zanaveskin, ChemInform abstract: catalytic hydrogenation of alkyne and alkadiene impurities in alkenes. practical and theoretical aspects, *Russian Chemical Review*, 2009, **78**, 231, doi: 10.1002/chin.200938260.

[7] M. A. Stoffels, F. J. R. Klauck, T. Hamadi, F. Glorius, J.

© Engineered Science Publisher LLC 2024

Leker, Technology trends of catalysts in hydrogenation reactions: a patent landscape analysis, *Advanced Synthesis & Catalysis*, 2020, **362**, 1258-1274, doi: 10.1002/adsc.201901292.
[8] J. Zhang, H. Zhang, Y. Wu, C. Liu, Y. Huang, W. Zhou, B. Zhang, Single-atom catalysts for thermal- and electro-catalytic hydrogenation reactions, *Journal of Materials Chemistry A*, 2022, **10**, 5743-5757, doi: 10.1039/d1ta07910g.
[9] F. Zaera, The surface chemistry of metal-based hydrogenation catalysis, *ACS Catalysis*, 2017, **7**, 4947-4967, doi: 10.1021/acscatal.7b01368.
[10] L. R. Redfern, Z. Li, X. Zhang, O. K. Farha, Highly selective acetylene semihydrogenation catalyzed by Cu nanoparticles supported in a metal–organic framework, *ACS Applied Nano Materials*, 2018, **1**, 4413-4417, doi: 10.1021/acsanm.8b01397.
[11] M. Takht Ravanchi, S. Sahebdelfar, S. Komeili, Acetylene selective hydrogenation: a technical review on catalytic aspects, *Reviews in Chemical Engineering*, 2018, **34**, 215-237, doi: 10.1515/revce-2016-0036.
[12] A. Borodziński, G. C. Bond, Selective hydrogenation of ethyne in ethene-rich streams on palladium catalysts, part 2: steady-state kinetics and effects of palladium particle size, carbon monoxide, and promoters, *Catalysis Reviews*, 2008, **50**, 379-469, doi: 10.1080/01614940802142102.
[13] T. D. Shittu, O. B. Ayodele, Catalysis of semihydrogenation of acetylene to ethylene: current trends, challenges, and outlook, *Frontiers of Chemical Science and Engineering*, 2022, **16**, 1031-1059, doi: 10.1007/s11705-021-2113-3.
[14] A. Sárkány, Formation of C4 Oligomers in Hydrogenation of Acetylene over Pd/Al_2O_3 and Pd/TiO_2 Catalysts, *Reaction Kinetics and Catalysis Letters,* 2001, **74**, 299-307, doi: 10.1023/A:1017945313041.
[15] J. Gu, M. Jian, L. Huang, Z. Sun, A. Li, Y. Pan, J. Yang, W. Wen, W. Zhou, Y. Lin, H.-J. Wang, X. Liu, L. Wang, X. Shi, X. Huang, L. Cao, S. Chen, X. Zheng, H. Pan, J. Zhu, S. Wei, W.-X. Li, J. Lu, Synergizing metal–support interactions and spatial confinement boosts dynamics of atomic nickel for hydrogenations, *Nature Nanotechnology*, 2021, **16**, 1141-1149, doi: 10.1038/s41565-021-00951-y.
[16] S. Wang, J. Zhu, J. Si, G. Zhao, Y. Liu, Y. Lu, High-performance Pd/brass-fiber catalyst for selective hydrogenation of acetylene: effect of calcination-assisted endogenous growth of ZnO-CuOx on brass-fiber, *Journal of Catalysis*, 2020, **382**, 295-304, doi: 10.1016/j.jcat.2019.12.027.
[17] P. Albers, J. Pietsch, S. F. Parker, Poisoning and deactivation of palladium catalysts, *Journal of Molecular Catalysis A: Chemical*, 2001, **173**, 275-286, doi: 10.1016/s1381-1169(01)00154-6.
[18] G. Vilé, D. Albani, N. Almora-Barrios, N. López, J. Pérez-Ramírez, Advances in the design of nanostructured catalysts for selective hydrogenation, *ChemCatChem*, 2016, **8**, 21-33, doi: 10.1002/cctc.201501269.
[19] X.-T. Li, L. Chen, C. Shang, Z.-P. Liu, *In situ* surface structures of PdAg catalyst and their influence on acetylene semihydrogenation revealed by machine learning and experiment, *Journal of the American Chemical Society*, 2021, **143**, 6281-6292, doi: 10.1021/jacs.1c02471.
[20] K. Kovnir, M. Armbrüster, D. Teschner, T. V. Venkov, L. Szentmiklósi, F. C. Jentoft, A. Knop-Gericke, Y. Grin, R. Schlögl, *In situ* surface characterization of the intermetallic compound PdGa–A highly selective hydrogenation catalyst, *Surface Science*, 2009, **603**, 1784-1792, doi: 10.1016/j.susc.2008.09.058.
[21] J. Feng, Y. Liu, M. Yin, Y. He, J. Zhao, J. Sun, D. Li, Preparation and structure-property relationships of supported trimetallic PdAuAg catalysts for the selective hydrogenation of acetylene, *Journal of Catalysis*, 2016, **344**, 854-864, doi: 10.1016/j.jcat.2016.08.003.
[22] T. Yang, Y. Feng, R. Ma, Q. Li, H. Yan, Y. Liu, Y. He, J. T. Miller, D. Li, Improvement of selectivity in acetylene hydrogenation with comparable activity over ordered PdCu catalysts induced by post-treatment, *ACS Applied Materials & Interfaces*, 2021, **13**, 706-716, doi: 10.1021/acsami.0c19329.
[23] M. R. Ball, K. R. Rivera-Dones, E. B. Gilcher, S. F. Ausman, C. W. Hullfish, E. A. Lebrón, J. A. Dumesic, AgPd and CuPd catalysts for selective hydrogenation of acetylene, *ACS Catalysis*, 2020, **10**, 8567-8581, doi: 10.1021/acscatal.0c01536.
[24] M. Hu, S. Zhao, S. Liu, C. Chen, W. Chen, W. Zhu, C. Liang, W.-C. Cheong, Y. Wang, Y. Yu, Q. Peng, K. Zhou, J. Li, Y. Li, MOF-confined sub-2 nm atomically ordered intermetallic PdZn nanoparticles as high-performance catalysts for selective hydrogenation of acetylene, *Advanced Materials*, 2018, **30**, 1801878, doi: 10.1002/adma.201801878.
[25] M. Kuhn, M. Lucas, P. Claus, Long-time stability vs deactivation of $Pd–Ag/Al_2O_3$ egg-shell catalysts in selective hydrogenation of acetylene, *Industrial & Engineering Chemistry Research*, 2015, **54**, 6683-6691, doi: 10.1021/acs.iecr.5b01682.
[26] A. Borodziński, Hydrogenation of acetylene–ethylene mixtures on a commercial palladium catalyst, *Catalysis Letters*, 1999, **63**, 35-42, doi: 10.1023/A:1019052618049.
[27] O. Dehghani, M. R. Rahimpour, A. Shariati, An experimental approach on industrial Pd-Ag supported α-Al_2O_3 catalyst used in acetylene hydrogenation process: mechanism, kinetic and catalyst decay, *Processes*, 2019, **7**, 136, doi: 10.3390/pr7030136.
[28] M. Kanai, M. Beller, Introduction to hybrid catalysis, *Organic & Biomolecular Chemistry*, 2021, **19**, 702-704, doi: 10.1039/d0ob90177f.
[29] J. Bu, Z. Liu, W. Ma, L. Zhang, T. Wang, H. Zhang, Q. Zhang, X. Feng, J. Zhang, Selective electrocatalytic semihydrogenation of acetylene impurities for the production of polymer-grade ethylene, *Nature Catalysis*, 2021, **4**, 557-564, doi: 10.1038/s41929-021-00641-x.
[30] S. Wang, K. Uwakwe, L. Yu, J. Ye, Y. Zhu, J. Hu, R. Chen,

 © Engineered Science Publisher LLC 2024

Z. Zhang, Z. Zhou, J. Li, Z. Xie, D. Deng, Highly efficient ethylene production via electrocatalytic hydrogenation of acetylene under mild conditions, *Nature Communications*, 2021, **12**, 7072, doi: 10.1038/s41467-021-27372-8.
[31] D. A. Outka, C. M. Friend, S. Jorgensen, R. J. Madix, Adsorption and hydrogenation of acetylene on copper Cu(110) and Cu(110)-O surfaces, *Journal of the American Chemical Society*, 1983, **105**, 3468-3472, doi: 10.1021/ja00349a016.
[32] Z. H. Zhang, H. J. Zhu, C. H. Zhou, H. Wang, Geopolymer from Kaolin in China: an overview, *Applied Clay Science*, 2016, **119**, 31-41, doi: 10.1016/j.clay.2015.04.023.
[33] F. Bin, C. Song, G. Lv, J. Song, K. Wang, X. Li, Soot low-temperature combustion on Cu–Zr/ZSM-5 catalysts in O2/He and NO/O2/He atmospheres, *Proceedings of the Combustion Institute*, 2013, **34**, 2303-2311, doi: 10.1016/j.proci.2012.07.075.
[34] C. Riley, A. De La Riva, S. Zhou, Q. Wan, E. Peterson, K. Artyushkova, M. D. Farahani, H. B. Friedrich, L. Burkemper, N.-V. Atudorei, S. Lin, H. Guo, A. Datye, Synthesis of nickel-doped ceria catalysts for selective acetylene hydrogenation, *ChemCatChem*, 2019, **11**, 1526-1533, doi: 10.1002/cctc.201801976.
[35] B. Zhang, Y. Hou, Z. Yu, Y. Liu, J. Huang, L. Qian, J. Xiong, Three-dimensional electro-Fenton degradation of Rhodamine B with efficient Fe-Cu/Kaolin particle electrodes: Electrodes optimization, kinetics, influencing factors and mechanism, *Separation and Purification Technology*, 2019, **210**, 60-68, doi: 10.1016/j.seppur.2018.07.084.
[36] J. Wang, Y. Wu, Y. Cao, G. Li, Y. Liao, Influence of surface roughness on contact angle hysteresis and spreading work, *Colloid and Polymer Science*, 2020, **298**, 1107-1112, doi: 10.1007/s00396-020-04680-x.
[37] T. M. Ivanova, K. I. Maslakov, A. A. Sidorov, M. A. Kiskin, R. V. Linko, S. V. Savilov, V. V. Lunin, I. L. Eremenko, XPS detection of unusual Cu(II) to Cu(I) transition on the surface of complexes with redox-active ligands, *Journal of Electron Spectroscopy and Related Phenomena*, 2020, **238**, 146878, doi: 10.1016/j.elspec.2019.06.010.
[38] M. Tejeda-Serrano, M. Mon, B. Ross, F. Gonell, J. Ferrando-Soria, A. Corma, A. Leyva-Pérez, D. Armentano, E. Pardo, Isolated Fe(III)–O sites catalyze the hydrogenation of acetylene in ethylene flows under front-end industrial conditions, *Journal of the American Chemical Society*, 2018, **140**, 8827-8832, doi: 10.1021/jacs.8b04669.
[39] S. Zhou, L. Kang, X. Zhou, Z. Xu, M. Zhu, Pure acetylene semihydrogenation over Ni–Cu bimetallic catalysts: effect of the Cu/Ni ratio on catalytic performance, *Nanomaterials*, 2020, **10**, 509, doi: 10.3390/nano10030509.
[40] S. Hu, C. Zhang, M. Wu, R. Ye, D. Shi, M. Li, P. Zhao, R. Zhang, G. Feng, Semi-hydrogenation of acetylene to ethylene catalyzed by bimetallic CuNi/ZSM-12 catalysts, *Catalysts*, 2022, **12**, 1072, doi: 10.3390/catal12091072.
[41] D. Wang, R. Ye, C. Zhang, C. Jin, Z.-H. Lu, M. Shakouri, B. Han, T. Wang, Y. Zhang, R. Zhang, Y. Hu, J. Zhou, G. Feng, Robust Ni_xSn/ZSM-12 catalysts with zeolite as the support and Sn as the promoter for acetylene semi-hydrogenation, *Energy & Fuels*, 2023, **37**, 13305-13318, doi: 10.1021/acs.energyfuels.3c01891.
[42] O. Matselko, R. R. Zimmermann, A. Ormeci, U. Burkhardt, R. Gladyshevskii, Y. Grin, M. Armbrüster, Revealing electronic influences in the semihydrogenation of acetylene, *The Journal of Physical Chemistry C*, 2018, **122**, 21891-21896, doi: 10.1021/acs.jpcc.8b05732.
[43] F. Huang, Y. Deng, Y. Chen, X. Cai, M. Peng, Z. Jia, P. Ren, D. Xiao, X. Wen, N. Wang, H. Liu, D. Ma, Atomically dispersed Pd on nanodiamond/graphene hybrid for selective hydrogenation of acetylene, *Journal of the American Chemical Society*, 2018, **140**, 13142-13146, doi: 10.1021/jacs.8b07476.
[44] Y. Liu, Y. He, D. Zhou, J. Feng, D. Li, Catalytic performance of Pd-promoted Cu hydrotalcite-derived catalysts in partial hydrogenation of acetylene: effect of Pd–Cu alloy formation, *Catalysis Science & Technology*, 2016, **6**, 3027-3037, doi: 10.1039/c5cy01516b.
[45] Y. Luo, S. Alarcón Villaseca, M. Friedrich, D. Teschner, A. Knop-Gericke, M. Armbrüster, Addressing electronic effects in the semi-hydrogenation of ethyne by InPd2 and intermetallic Ga–Pd compounds, *Journal of Catalysis*, 2016, **338**, 265-272, doi: 10.1016/j.jcat.2016.03.025.
[46] T. Yang, Y. Feng, R. Ma, Q. Li, H. Yan, Y. Liu, Y. He, J. T. Miller, D. Li, Improvement of selectivity in acetylene hydrogenation with comparable activity over ordered PdCu catalysts induced by post-treatment, *ACS Applied Materials & Interfaces*, 2021, **13**, 706-716, doi: 10.1021/acsami.0c19329.
[47] G. X. Pei, X. Y. Liu, A. Wang, A. F. Lee, M. A. Isaacs, L. Li, X. Pan, X. Yang, X. Wang, Z. Tai, K. Wilson, T. Zhang, Ag alloyed Pd single-atom catalysts for efficient selective hydrogenation of acetylene to ethylene in excess ethylene, *ACS Catalysis*, 2015, **5**, 3717-3725, doi: 10.1021/acscatal.5b00700.
[48] R. Ma, Y. He, J. Feng, Z.-Y. Hu, G. Van Tendeloo, D. Li, A facile synthesis of Ag@PdAg core-shell architecture for efficient purification of ethene feedstock, *Journal of Catalysis*, 2019, **369**, 440-449, doi: 10.1016/j.jcat.2018.11.037.
[49] G. X. Pei, X. Y. Liu, X. Yang, L. Zhang, A. Wang, L. Li, H. Wang, X. Wang, T. Zhang, Performance of Cu-alloyed Pd single-atom catalyst for semihydrogenation of acetylene under simulated front-end conditions, *ACS Catalysis*, 2017, **7**, 1491-1500, doi: 10.1021/acscatal.6b03293.
[50] J. Osswald, K. Kovnir, M. Armbruster, R. Giedigkeit, R. Jentoft, U. Wild, Y. Grin, R. Schlogl, Palladium–gallium intermetallic compounds for the selective hydrogenation of acetylenePart II: surface characterization and catalytic performance, *Journal of Catalysis*, 2008, **258**, 219-227, doi: 10.1016/j.jcat.2008.06.014.
[51] L. Shao, W. Zhang, M. Armbrüster, D. Teschner, F. Girgsdies, B. Zhang, O. Timpe, M. Friedrich, R. Schlögl, D. S. Su, Nanosizing intermetallic compounds onto carbon nanotubes: active and selective hydrogenation catalysts, *Angewandte Chemie International Edition*, 2011, **50**, 10231-

© Engineered Science Publisher LLC 2024

10235, doi: 10.1002/anie.201008013.
[52] B. Mattson, W. Foster, J. Greimann, T. Hoette, N. Le, A. Mirich, S. Wankum, A. Cabri, C. Reichenbacher, E. Schwanke, Heterogeneous catalysis: the horiuti–polanyi mechanism and alkene hydrogenation, *Journal of Chemical Education*, 2013, **90**, 613-619, doi: 10.1021/ed300437k.

Publisher's Note: Engineered Science Publisher remains neutral with regard to jurisdictional claims in published maps and institutional affiliations.

 © Engineered Science Publisher LLC 2024